11-2016

Gear Tooth Mesh Stiffness: A Comparison of Calculation Approaches

Christopher G. Cooley
Department of Mechanical Engineering and Energy Processes, chris.cooley@siu.edu

Chunguang Liu
University of Michigan-Shanghai Jiao Tong University Joint Institute

Xiang Dai
Virginia Tech

Robert G. Parker
Virginia Tech

Recommended Citation
Cooley, Christopher G., Liu, Chunguang, Dai, Xiang and Parker, Robert G. "Gear Tooth Mesh Stiffness: A Comparison of Calculation Approaches." *Mechanism and Machine Theory* 105 (Nov 2016): 540–553. doi:10.1016/j.mechmachtheory.2016.07.021.

Gear Tooth Mesh Stiffness: A Comparison of Calculation Approaches

Christopher G. Cooley[a], Chunguang Liu[b], Xiang Dai[c], Robert G. Parker[c,d]

[a] *Southern Illinois University Carbondale, Carbondale, IL 62901*
[b] *University of Michigan-Shanghai Jiao Tong University Joint Institute, Shanghai Jiao Tong University, Shanghai, China 200240*
[c] *Department of Mechanical Engineering, Virginia Tech, Blacksburg, VA 24061, USA*
[d] *L. S. Randolph Professor*

Abstract

This work compares spur gear tooth mesh stiffness calculations using two approaches. The first is a common approach from the literature that calculates the mesh stiffness by dividing the mesh force by the mesh deflection, which we call the average slope method. The second approach calculates the local slope of the force-deflection curve about a nominal deflection. The two approaches result in meaningfully different mesh stiffness predictions that persist for wide ranges of applied torque and for gear teeth with tooth surface modifications. It is shown that each calculation approach has its own distinct use, broadly divided as average slope mesh stiffness for static analyses and local slope for dynamic analyses. Furthermore, the two stiffness calculation approaches lead to different vibration models. This means for vibration analyses the choice is not solely which of the two stiffnesses to use but also how to implement that stiffness appropriately in a model. Even though the mesh stiffnesses in this work are calculated using a finite element/contact mechanics approach, the findings are equally valid for mesh stiffnesses obtained from conventional finite element methods, analytical models, and experiments.

Keywords: Tooth mesh stiffness, Spur gears, Gear tooth modifications, Finite element/contact mechanics, Gear vibration

*Corresponding author
Email addresses: chris.cooley@siu.edu (Christopher G. Cooley), r.parker@vt.edu (Robert G. Parker)

1. Introduction

Tooth mesh stiffness waveforms are used as inputs to analytical models for gear vibrations in Refs. [1, 2, 3, 4, 5, 6, 7, 8, 9, 10] for gear pairs, Refs. [11, 12, 13, 14, 15] for idler gears, and Refs. [16, 17, 18, 19, 20, 21, 22, 23, 24, 25] for planetary gears, for example. The accuracy of these models largely depends on the accuracy of the tooth mesh stiffness representation.

Not all dynamic models for gear systems use pre-specified fluctuating mesh stiffnesses as inputs. Analytical gear vibration models in Refs. [26, 27, 28, 29, 30], for example, calculate the instantaneous tooth mesh stiffness at each time step as the gears rotate kinematically and vibrate.

Tooth mesh stiffnesses are usually calculated using computational models. A finite element/contact mechanics approach has been used to determine mesh stiffness fluctuations in Refs. [6, 19, 21, 22]. Chung et al. [31] calculated gear tooth mesh stiffnesses for varying design parameters using a finite element approach. Analytical models to calculate tooth mesh stiffness have been proposed in Refs. [5, 7, 31, 32]. Raghuwanshi and Parey [33] used photoelasticity to measure the mesh stiffness of gear teeth with cracks. It is possible to determine mesh stiffness from experiments by measuring angular gear deflections with high precision encoders.

This study compares two methods to calculate the tooth mesh stiffness and discusses the appropriate uses of each method for static and dynamic analyses. One method, called the local slope method, represents the tooth stiffness by the local slope of the usually nonlinear mesh force versus mesh deflection (or torque versus rotation) curve at a nominal tooth load. The second method, called the average slope method, is the commonly used method where the mesh stiffness is the total mesh force divided by the mesh deflection. Results are given for high and low applied torques, and for gears with and without tooth surface modifications. Differences between the methods are substantial.

We show that the average slope method is appropriate for static analyses (where the local slope method is incorrect), and the local slope method is appropriate for dynamic analyses of gears vibrating about a nominal static deflection (where the average slope method is inappropriate). Furthermore, it is not only a question of which mesh stiffness to use; the vibration model itself changes based on the choice of mesh stiffness. One can not simply exchange the average slope stiffness for local slope stiffness or vice versa in a given dynamic model. Example simulations demonstrate the findings.

2. Mesh Stiffness Calculation

Throughout this paper we demonstrate the mesh stiffness calculations using a spur gear pair from Refs. [34, 35]. The gears have 50 teeth, 3 mm module, 20 deg pressure angle, 4.64 mm tooth thickness, 140 mm root diameter, and 20 mm facewidth. The outer diameters are 154.41 mm for the pinion and 154.71 mm for the gear so that the (theoretical) involute contact ratio for the pair is 1.37. The gear blank inner diameters are 45 mm. The finite element/contact mechanics model of the gear pair is shown in Fig. 1. The model consists of the teeth and blanks for each gear. A torque is applied to the pinion (the input drive gear) at its inner surface marked "T", and the pinion rotation is calculated. The driven gear is constrained so that it has no rigid body rotation at surface "C" in Fig. 1, but points on this surface (and on the pinion surface marked "T" where the torque is applied) can deform elastically.

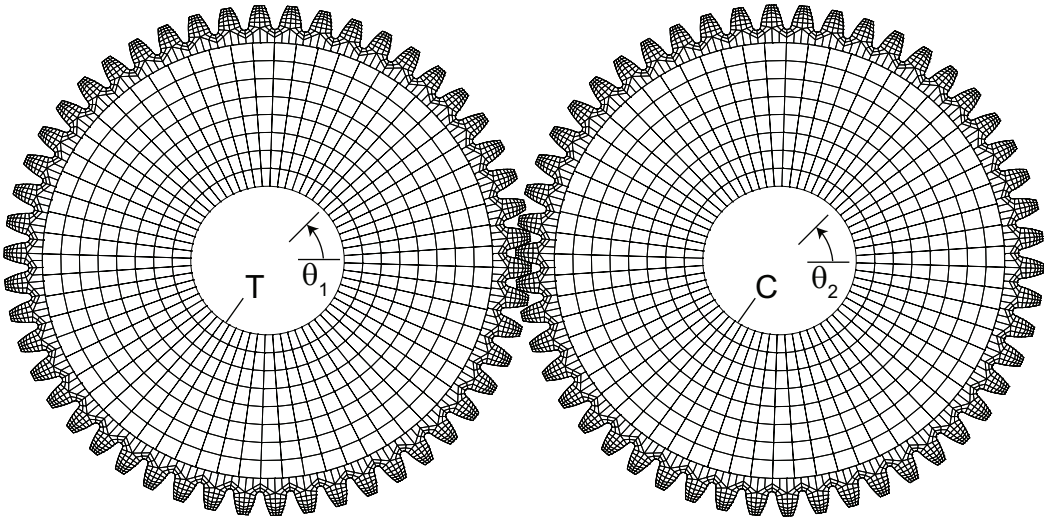

Figure 1: Finite element model of the spur gear pair used in this work. A torque is applied to the pinion's inner cylindrical surface denoted by "T". The inner cylindrical surface at "C" is constrained so that the gear has no rigid body rotation, although points on this surface (and on the surface marked "T") can deform elastically.

For multi-mesh systems, like idler and planetary gears, the mesh stiffness for each pair of gears in mesh (e.g., the sun and a planet gear) would be calculated separately using a model of only that gear pair. When these mesh

stiffnesses are assembled into a system model, the phase of each mesh must be properly included [13, 36, 37].

The force-deflection curve for gear teeth is nonlinear because of elastic contact between the mating gear teeth. An example force-deflection curve is shown in Fig. 2 for the spur gear pair (defined above) with two tooth pairs in contact. Figure 2 represents a single point in the mesh cycle. The force-deflection behavior will vary at each point of the mesh cycle, with the most dramatic change occurring when the number of teeth in contact changes. Nevertheless, the character of the force-deflection relationship at each point will be similar to Fig. 2. The gear teeth have small deflection for vanishing applied torque (i.e., unloaded transmission error) because of profile modification. The curve exhibits classical hardening behavior associated with the growth of the contact area as applied load increases. The stiffness of the gear teeth is calculated from curves like these using the two approaches described below.

The aim of this work is to accurately represent the elastic behavior of the contacting gear teeth shown in Fig. 2 using discrete stiffness elements. The calculated discrete stiffnesses can be applied to lumped-parameter models with rotations and translations, continuous models, and finite element models where the contacting gear teeth are represented as discrete stiffnesses.

2.1. Average slope approach

The tooth mesh stiffness has been calculated by dividing the mesh force by the mesh deflection in Refs. [3, 4, 5, 6, 9, 19, 24, 25, 31, 38, 39, 40, 32, 33, 41], for example. We refer to this as the average slope approach. The gears are analyzed statically for a number of different gear configurations over one mesh cycle to capture the effects caused by changing contact conditions. The mesh stiffness at each point in the mesh cycle is

$$k_a = \frac{F_m}{q_m}, \tag{1}$$

where the mesh deflection $q_m = r_{b1}\theta_1 + r_{b2}\theta_2 - \epsilon$, $r_{b1,b2}$ are the gear base radii, $\theta_{1,2}$ are the absolute gear rotational deflections, i.e., the "rigid body" rotational motion of the gears, measured relative to the perfectly conjugate gear motion, and $F_m = T_1/r_{b1} = T_2/r_{b2}$ is the tooth mesh force. The quantity $r_{b1}\theta_1 + r_{b2}\theta_2$ is commonly called the loaded transmission error. The unloaded transmission error ϵ is from tooth surface modifications. For unmodified gear teeth ϵ vanishes. For vanishing applied load the static transmission error

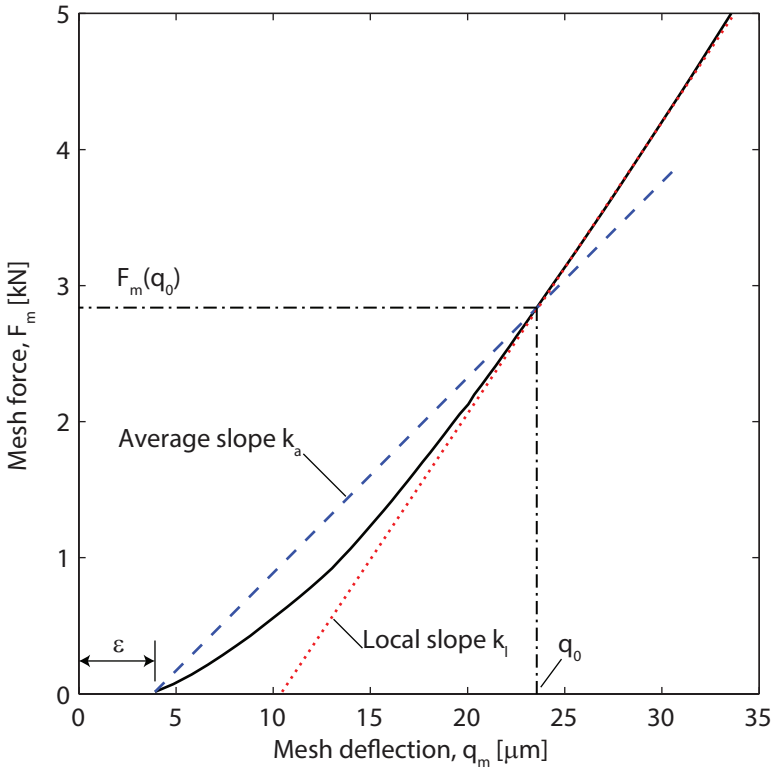

Figure 2: Finite element calculation of the force-deflection curve for the gear mesh. Both gears have modified teeth with 10 μm of linear tip relief that starts at 20.9 deg roll angle (i.e., the pitch point) and ends at the tooth tip, and 20 μm of symmetric lead crown.

becomes the unloaded transmission error, i.e., $r_{b1}\theta_1 + r_{b2}\theta_2 \rightarrow \epsilon$, so that the mesh deflection q_m vanishes. The rotational deflections $\theta_{1,2}$ could be directly measured by encoders in experiments. Finite element codes typically output the gear rotational deflections $\theta_{1,2}$. For finite element software that instead gives only the absolute elastic deflections of points on the finite element model, these rotations can be calculated by circumferentially averaging the absolute tangential deflections of points at a specified radius around the gear. In this case, one must choose a radius at which to calculate the average. Figure 3 shows the absolute tangential deflections of the gear and pinion calculated at multiple radii ranging from the inner diameters of Fig. 1 to near the root diameter using the finite element software Calyx. Table 1 shows the averaged tangential deflections, rotations $\theta_{1,2}$ calculated from the averages, and the mesh deflections calculated from the rotations. The results show that while minor differences occur in the rotational deflections calculated at different radii, the mesh deflections, and so the resulting mesh stiffnesses, are insensitive to the radius where the absolute tangential deflections are averaged. The mesh deflections in Table 1 agree exactly with the mesh deflection $q_m = 12.381941\ \mu m$ produced as a direct output of the finite element code using the gear "rigid body" rotational deflections.

Table 1: Finite element calculation of the circumferentially averaged absolute tangential deflections U_θ, rotational deflections $\theta = U_\theta/r$, and mesh deflections $q_m = r_{b1}\theta_1 + r_{b2}\theta_2$ ($\epsilon = 0$ because the gear teeth are unmodified) calculated from the rotations at varying radii. The applied torque is 170 Nm.

	Pinion		Gear		
Radius, r [mm]	U_θ [μm]	θ_1 [rad]	U_θ [μm]	θ_2 [rad]	q_m [μm]
22.5	3.650	1.62230×10^{-4}	-0.3028	-1.34581×10^{-5}	12.381941
44.25	7.196	1.62620×10^{-4}	-0.5782	-1.30675×10^{-5}	12.381941
60.5625	9.780	1.61486×10^{-4}	-0.8601	-1.42023×10^{-5}	12.381941

The stiffness from the average slope approach expressed in Eq. (1) is illustrated by the dashed (blue) line in Fig. 2. Thus, at each point of the mesh cycle stiffness from the average slope approach is the slope of a line extending from the deflection ϵ at zero mesh force to the point on the curve corresponding to the force and deflection values for the given torque; this is the average stiffness over the deflection range beginning from zero torque to the final deflection for the given torque.

Figure 4 illustrates the differences between the loaded transmission error,

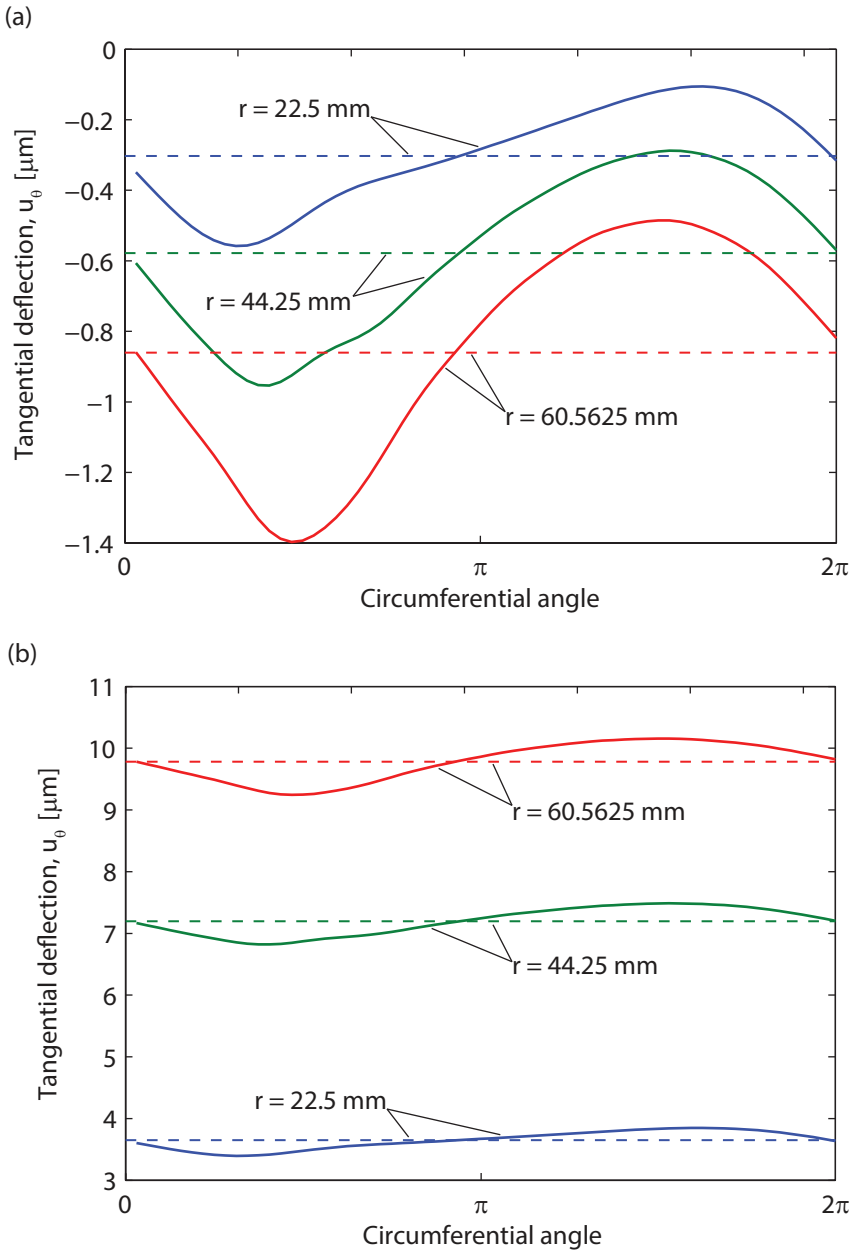

Figure 3: Finite element calculation of the circumferential variation in the absolute tangential deflections of the (a) gear and (b) pinion at varying radii. The circumferentially averaged values are shown by dashed horizontal lines. The applied torque is 170 Nm.

unloaded transmission error, and mesh deflection for the example gear pair with 10 μm of linear tip relief starting at 20.9 deg roll angle (which corresponds to the pitch point) and ending at the tip of the tooth. The loaded static transmission error (solid line) has small fluctuations over the mesh cycle, so these modifications may be a good choice for reducing vibration. The unloaded transmission error (dashed line) vanishes at the beginning of the mesh cycle, which corresponds to pitch point contact. The unloaded transmission error increases linearly up to 0.5 mesh cycle because linear tip relief is applied starting at the pitch point. Above 0.5 mesh cycle the unloaded transmission error decreases back to zero as the contact location approaches the pitch point on the next tooth. The deflection in the mesh (dotted line) is the difference between the loaded and unloaded transmission error. This is the quantity used to calculate mesh stiffness using the average slope approach.

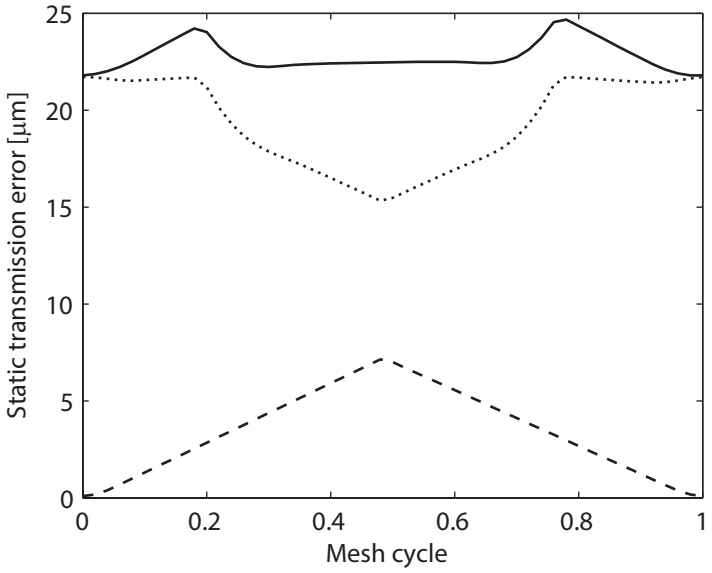

Figure 4: Finite element calculation of loaded static transmission error (solid), unloaded transmission error (dashed), and mesh deflection (dotted) over one mesh cycle. The gear teeth have 10 μm of linear tip relief that starts at 20.9 deg roll angle (i.e., the pitch point) and ends at the tooth tip.

2.2. Local slope approach

In this approach the tooth stiffness is the local slope of the force-deflection curve at some nominal deflection q_m (red, dotted line in Fig. 2). The local

slope of this curve using first-order finite difference approximation gives the mesh stiffness

$$k_l = \frac{F_m(q_m + \Delta q_m) - F_m(q_m - \Delta q_m)}{2\Delta q_m}, \tag{2}$$

where the parentheses indicate the deflection values where the force is calculated (rather than multiplication of the force and deflection quantities), Δq_m is a specified small change in mesh deflection, and F_m is calculated from the model. This process yields the stiffness as the slope of the red, dotted line in Fig. 2 representing the local slope of the force versus deflection curve for a given force or given deflection. This approach was used to calculate the stiffnesses of rolling element bearings in Ref. [42].

It is convenient to instead calculate the mesh compliance $c_l = k_l^{-1} = \big[q_m(F_m + \Delta F_m) - q_m(F_m - \Delta F_m)\big]/2\Delta F_m$, as opposed to directly calculating stiffness. Here, ΔF_m is mesh force step size. In this way the input torque (i.e., the mesh force) of the gears is specified and the gear deflections are calculated.

The displacement (Δq_m) or mesh force (ΔF_m) step size for the finite difference calculation must be carefully chosen. Excellent convergence was obtained using a step size of 1% of the nominal torque for the gear pair analyzed in this study. Higher-order finite difference expressions yield no additional accuracy for stiffness calculations using the finite element/contact mechanics method [42].

To calculate the mesh stiffness using the average slope approach for unmodified gears one simulation at the operating torque is necessary. For teeth with modifications an additional simulation at very low torque is necessary to calculate the unloaded transmission error ϵ. Calculation of mesh stiffness using the local slope approach in Eq. (2) requires two simulations: one above the nominal deflection or load, and another below it. In terms of computation time, the local slope approach is no different than the average slope approach when the gear teeth have modifications.

3. Results

We illustrate the differences between the two mesh stiffness calculation approaches using a finite element/contact mechanics model [43]. This formulation calculates the tooth contact at each configuration within a mesh cycle due to the precise tooth surface geometry (which is modeled with negligible

geometric error using an extremely large number of points in a geometric mesh that is distinct from the finite element node points) and elastic deformations. There are no *a priori* assumptions or specifications of the tooth contact distribution. The finite element/contact mechanics formulation has been shown to accurately predict the dynamic response of gear pairs in Refs. [6, 9, 44], the dynamic tooth root strains of gear pairs in Ref. [45], and the tooth root strains in the ring gears of planetary gears in Ref. [46]. Similar differences between the mesh stiffness calculations are expected using other finite element approaches, analytical models, and experiments.

Figure 5 compares the two mesh stiffness calculations over one tooth mesh cycle and their spectra for an applied torque of 300 Nm and unmodified tooth surfaces. The tooth cycle is divided into regions where one pair of teeth is in contact and two pairs of teeth are in contact. The vertical lines in Fig. 5 that separate these regions are found from the finite element/contact mechanics model. The high stiffness region extends over a range of the mesh cycle that is larger than expected for this 1.37 contact ratio gear pair due to the large applied load causing premature corner contact in the absence of profile modifications. The stiffness is meaningfully larger when two pairs of teeth are in contact, an expected feature that is captured in both approaches. This fluctuation in stiffness excites vibration in spur gear systems [1, 2]. Within each region (but away from 0.2 and 0.8 mesh cycle) both approaches predict only small changes in stiffness due to changing contact conditions (but not changes in the number of teeth in contact). The local slope approach results in larger stiffness predictions than the average slope approach over the entire mesh cycle. This difference is due to the nonlinear hardening behavior associated with elastic contact. It is consistent with the differences expected from the force-deflection curve in Fig. 2. The mean mesh stiffnesses over a complete mesh cycle for the average and local slope approaches are 238.4 $N/\mu m$ and 252.3 $N/\mu m$, respectively. This corresponds to a 5.6% difference.

The two approaches differ greatly near 0.2 and 0.8, where the number of gear tooth pairs in contact changes. These regions are where, in the absence of profile modifications, premature corner tooth contact occurs due to elastic tooth defections. The average slope approach has sloped ramp-like regions that connect the low stiffness to the high stiffness. In the local slope approach, however, there are sharp jumps in stiffness near 0.17 and 0.80. The local slope approach predicts the gear mesh has large stiffness for the entire range of double tooth contact, even if some of that contact is corner tooth contact. This makes sense physically; the unintended premature

corner contact creates a second pair of contacting teeth that adds substantial mesh stiffness. These sharp differences are responsible for the differences in the spectra (Fig. 5(b)). The local slope approach generally leads to larger amplitudes for the higher harmonics. In gear dynamic models that use mesh stiffness fluctuations like Refs. [2, 12, 13, 14, 17, 18, 20], these two approaches may lead to meaningfully different dynamic response and parametric instability regions.

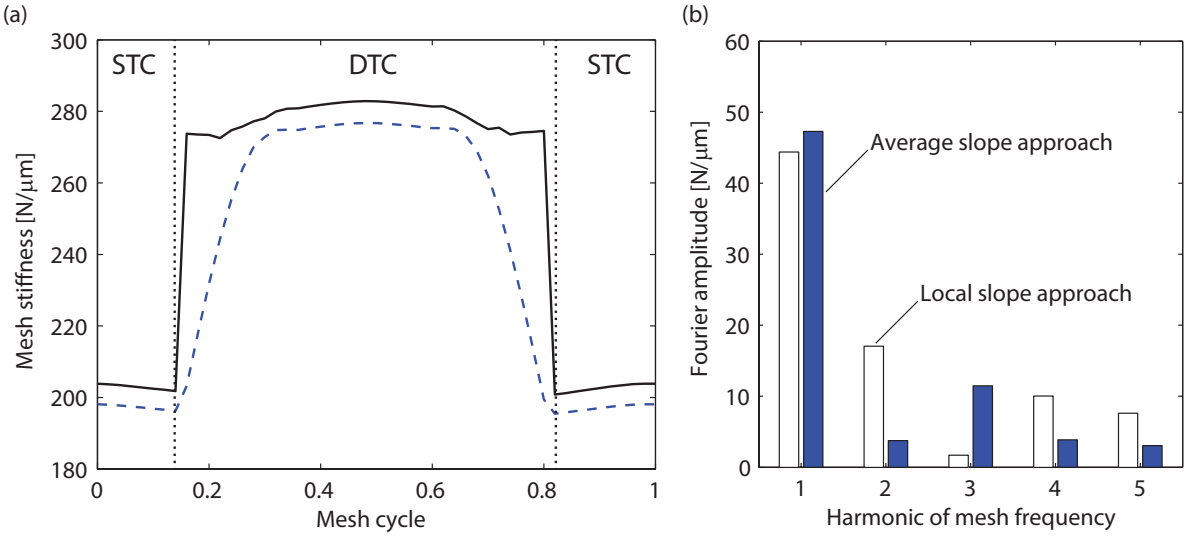

Figure 5: Finite element calculation of tooth mesh stiffness over one tooth mesh cycle for 300 Nm applied torque and unmodified teeth. The dashed (blue) and solid (black) lines denote the average and local slope approaches, respectively. Regions where a single pair (two pairs) of teeth are in contact are denoted by "STC" ("DTC") as determined by the finite element model.

The two mesh stiffness calculations are shown in Fig. 6 for gear teeth with 10 μm of linear tip relief starting at 20.9 deg roll angle and ending at the tooth tip. The local slope approach (solid, black line) has similar shape and amplitude as for the unmodified gears in Fig. 5. The duration of the larger amplitude stiffness region, where two tooth pairs are in contact, is smaller than for unmodified teeth (Fig. 5) due to the removal of some premature tooth contact by the profile modifications. The average slope approach is shown by the dashed (blue) line in Fig. 6. This curve is drastically different than that for unmodified teeth (dashed, blue line in Fig. 5). Between 0.2 to 0.8 mesh cycle in Fig. 6 (when two pairs of teeth are in contact) large

differences occur between the two approaches. In this region the unloaded transmission error (Fig. 4) is large. When only one pair of teeth is in contact (below 0.2 and above 0.8 mesh cycle), which corresponds to regions where the tooth modifications are small (Fig. 4), the average slope approach has similar relative behavior with the local slope approach as for unmodified gears in Fig. 5. The differences described above result in mesh stiffnesses with meaningfully different shape and spectra.

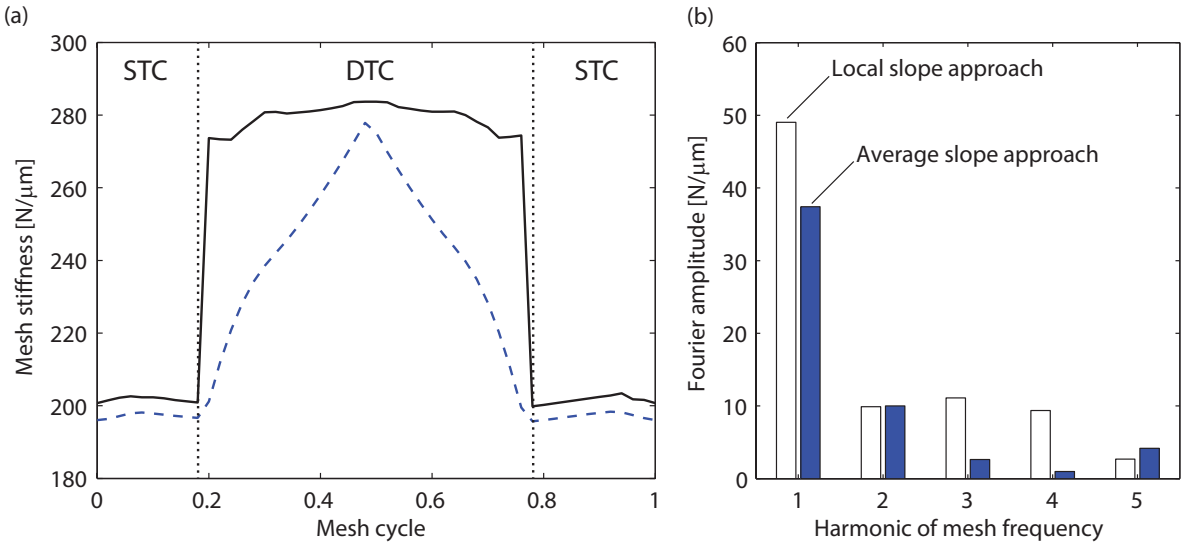

Figure 6: Finite element calculation of tooth mesh stiffness over one tooth pass cycle at 300 Nm applied torque. The gears have 10 μm of linear tip relief that starts at 20.9 deg roll angle (i.e., the pitch point) and ends at the tooth tip. The dashed (blue) and solid (black) lines denote the average and local slope approaches, respectively. Regions where a single pair (two pairs) of teeth are in contact are denoted by "STC" ("DTC") as determined by the finite element model.

To explain the differences observed between the average slope and local slope approaches in Figs. 5 and 6 we plot the force-deflection curves for these gears in Fig. 7 at multiple configurations within a mesh cycle. The solid curves are for unmodified teeth. The dashed curves are for linear profile modifications. The dotted horizontal line corresponds to the mesh force at 300 Nm applied torque. The solid (blue) curve at mesh cycle 0 has a single pair of teeth in contact and the solid (green) curve at mesh cycle 0.5 has two tooth pairs in contact. The solid (red) curve at 0.2 mesh cycle is for a configuration within the mesh cycle with a single pair of teeth in contact

at low load and deflection and two pairs of teeth in contact at high load. At low loads this curve has a slope nearly equal to that for a single pair of teeth in contact. At the instant a second pair of teeth come into contact the slope abruptly increases to a value nearly equal to that for two pairs of teeth in contact. The sharpness of the slope changes explains the jumps in mesh stiffness amplitudes seen in Fig. 5 near 0.2 and 0.8 mesh cycle. The local slope approach has stiffness amplitudes corresponding to contact of one pair and two pairs of teeth in contact. In contrast, the average slope approach mesh stiffness has ramp-like regions connecting the low and high stiffness regions in Fig. 5 because the slope of a line from the origin to a point above the transition to two pairs of teeth in contact for the solid red line changes gradually even though the local slope is nearly discontinuous. When the gear teeth have profile modifications (dashed curves in Fig. 7), the force-deflection curves have varying x-axis offsets due to the removal of material on the tooth profile from modifications. Otherwise, the force-deflection curves have similar behavior as that seen in the solid lines for unmodified teeth. The vastly different shape of the mesh stiffness in Fig. 6 using the average slope approach (dashed line) is due to the varying x-axis offset combined with the abrupt changes in slope that occur at the instant a second pair of teeth come into contact.

Figure 8 shows that the substantial differences between the two approaches observed above for 300 Nm occur for a wide range of applied torques.

The differences observed between the average and local slope mesh stiffness calculations for the 1.37 contact ratio gear pair occur for larger contact ratio gears, as seen in Fig. 9. This includes gear pairs that have contact ratios greater than two, where the number of pairs of gear teeth in contact changes between two and three. The gear and pinion in the 1.75 (2.01) contact ratio pair have 156 (156.98) mm outside diameters. The remaining parameters are identical to the 1.37 contact ratio gear pair.

Figure 10 shows that the amount of profile modifications substantially changes the mesh stiffness waveform and spectra predicted from each calculation approach. Figure 10a shows the range of high mesh stiffness predicted by the local slope approach depends on the amount of tooth profile modifications. This meaningfully changes the second and third harmonics of the mesh stiffness, but has little affect on the fundamental harmonic (Fig. 10b). All modification amounts result in stiffness curves with sharp jumps that mark the instants that the number of teeth in contact changes. These jumps do not occur when using the average slope approach for any amount of modification,

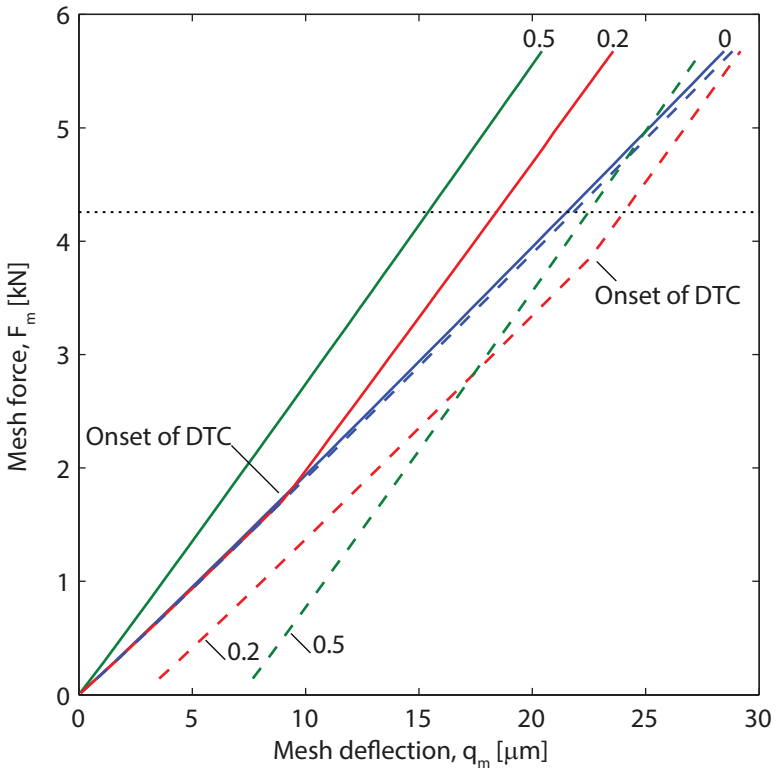

Figure 7: Finite element calculation of the force-deflection curves for the ICR 1.37 spur gear pair without modifications (solid lines) and 10 μm of linear tip modifications that starts at 20.9 deg starting roll angle (the pitch point) and ends at the tooth tip (dashed lines). The dotted horizontal line indicates the mesh force corresponding to 300 Nm torque. The numbers indicate the mesh cycle position.

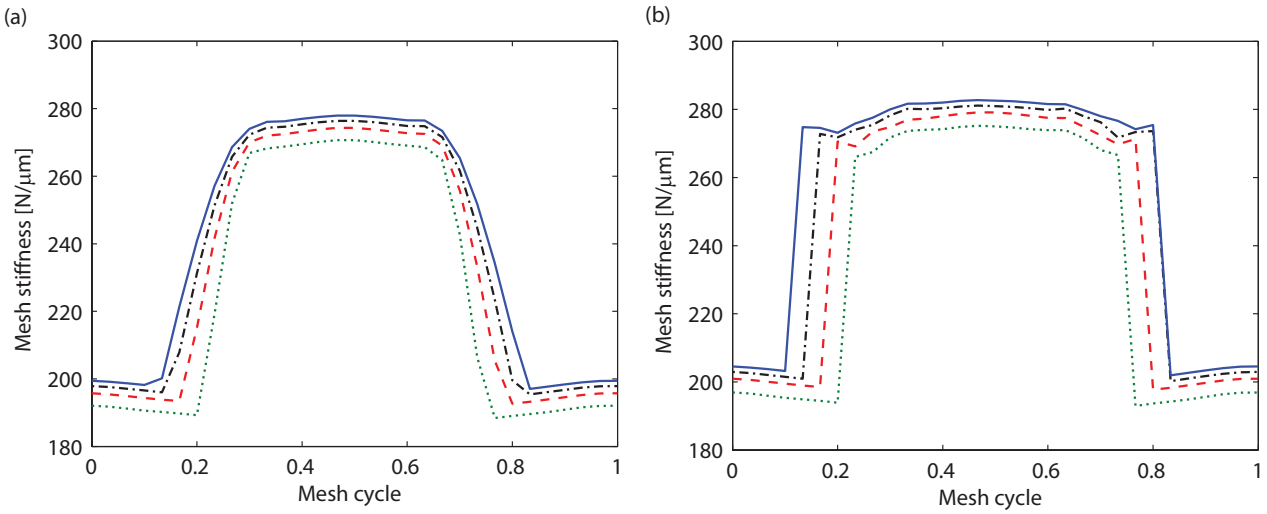

Figure 8: Finite element calculation of tooth mesh stiffness over one tooth mesh cycle for varying torque using the (a) average slope and (b) local slope approaches. The dotted (green), dashed (red), dash-dotted (black), and solid (blue) lines correspond to 100, 200, 300, and 400 Nm applied torque, respectively. The gear teeth are unmodified.

as seen in Fig. 10c. In the average slope approach the high stiffness region is almost entirely eliminated (Fig. 10c) even for modest amounts of modifications. Substantial differences are expected to occur if these stiffnesses were used as inputs to dynamic models because of their different spectra (Figs. 10b,d).

Figure 11 compares the local slope and average slope calculation of mesh stiffness for varying amounts of lead crown. Gear teeth with lead crown have decreased stiffness amplitudes compared to unmodified teeth because of the decreased contact area across the facewidth. The jumps between one and two tooth pairs in contact for the local slope approach are sharp but not discontinuous as they are without lead crown modifications. The local slope amplitude has substantially larger mean stiffness amplitudes than the average slope with the addition of lead crown, in agreement with expectations from the force-deflection behavior shown in Fig. 2.

4. Discussion

Here we show that each of the two mesh stiffness calculation approaches has its own distinct use. In summary, the average slope method (Eq. (1))

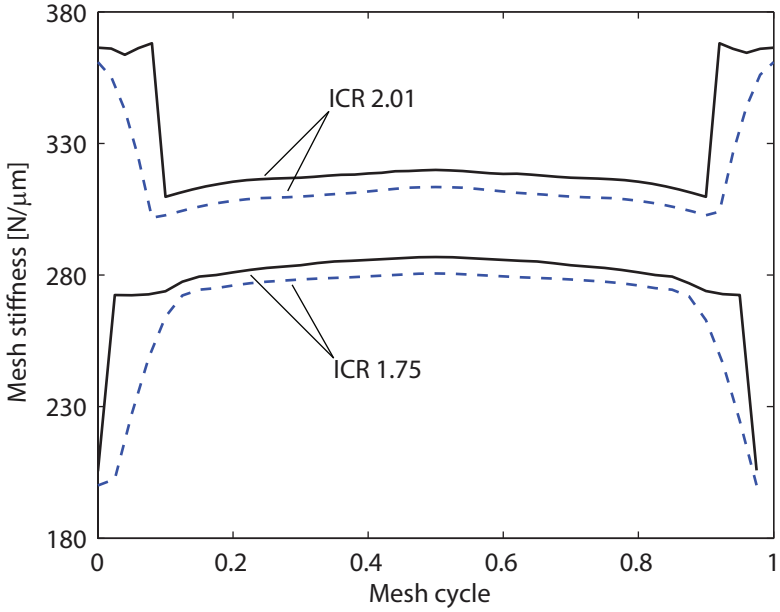

Figure 9: Finite element calculation of tooth mesh stiffness over one tooth mesh cycle for gear pairs with 1.75 and 2.01 (theoretical) contact ratios and unmodified teeth. The applied torque is 170 Nm. The solid (black) and dashed (blue) lines are the local and average slope calculations, respectively.

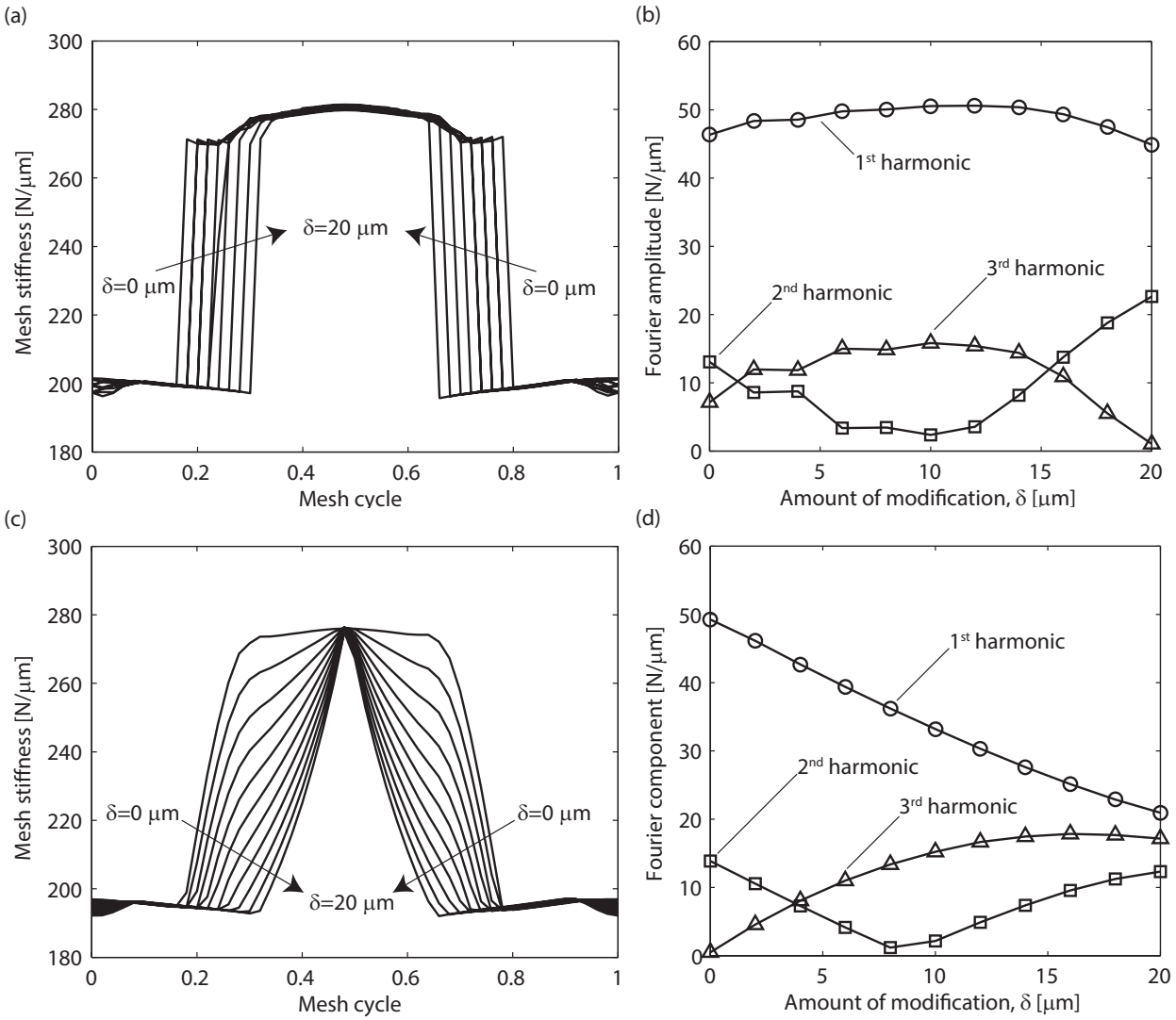

Figure 10: Finite element calculation of tooth mesh stiffness over one tooth pass cycle and its spectra for varying amount of linear tip relief using the local slope approach (a,b) and the average slope approach (c,d). In (b,d) the circle, square, and triangle markers correspond to the Fourier amplitudes of the first, second, and third harmonics of mesh frequency, respectively. The applied torque is 200 Nm.

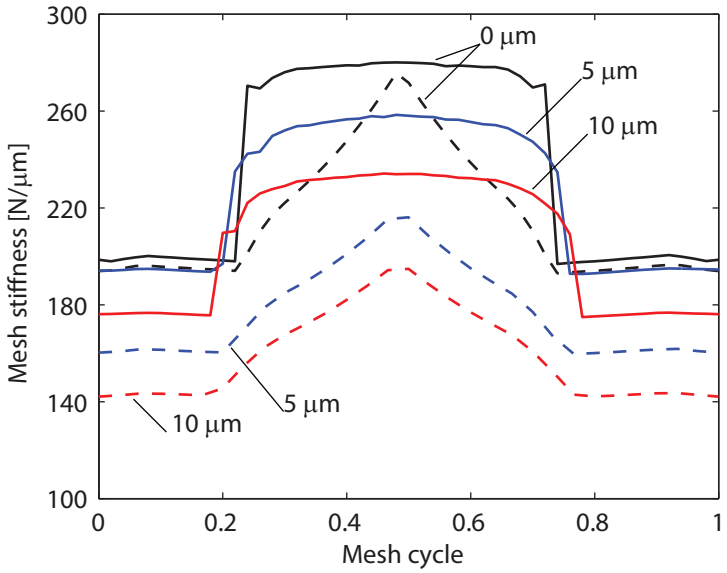

Figure 11: Finite element calculation of tooth mesh stiffness over one tooth pass cycle for varying amount of lead crown modification using the local slope approach (solid) and average slope approach (dashed). The teeth have 10 μm of linear tip relief that starts at 20.9 deg roll angle (i.e., the pitch point) and ends at the tooth tip. The applied torque is 200 Nm.

is appropriate when calculating static deflections relative to an unloaded state, such as for system windup or planetary gear load sharing. The local slope method (Eq. (2)) is appropriate when computing small deformations relative to a loaded state, such as for vibration analysis of loaded gears or static displacements relative to a loaded state caused by torque fluctuations.

For small mesh deflections about the nominal static deflection q_0 shown in Fig. 2, the mesh force at a particular point in the mesh cycle can be written as

$$F_m = F_m(q_0) + \left.\frac{\partial F_m}{\partial q_m}\right|_{q_m=q_0} (q_m - q_0) + O\left((q_m - q_0)^2\right), \tag{3}$$

where q_m is the instantaneous total mesh deflection and q_0 is the static transmission error. Both q_m and q_0 are total mesh deflections that include any contribution from unloaded transmission error ϵ. With use of Eqs. (1) and (2) and neglecting higher-order terms in the relative deflections Eq. (3) becomes

$$F_m = k_a(t)(q_0(t) - \epsilon(t)) + k_l(t)(q_m - q_0(t)), \tag{4}$$

where $k_a(t)$ is the average slope stiffness from Eq. (1) and $k_l(t)$ is the local slope stiffness from Eq. (2). Referring to Fig. 2, the first term in Eq. (4) is the force contribution from the dashed (blue) line, and the second term is that from the dotted (red) line. The quantities q_0, ϵ, k_a, and k_l all depend on the tooth contact conditions and therefore fluctuate periodically over a mesh cycle.

The concepts are evident for a single pair of gears with the force-deflection curve shown in Fig. 2. If the objective is to determine the total static deflection for a specified applied torque, then the average slope stiffness shown by the slope of the dashed blue line in Fig. 2 is needed and the relationship is given in Eq. (1). In this case, we need the linear stiffness that relates the instantaneous force to the deflection of the gears from their unloaded state; there is no need to consider the potentially nonlinear shape of the force-deflection curve between the unloaded and loaded states.

The local slope stiffness, however, is appropriate when analyzing small deflections of the gears relative to a loaded state. In these cases, one needs the local slope of the force-deflection curve evaluated at the loaded state, that is, the slope of the solid red line in Fig. 2. Conversely, the local slope stiffness is inappropriate to calculate the total deflection for specified applied

torque. Use of the local slope stiffness in this way would be representing the force versus deflection behaivor as a straight line through the origin with slope equal to that of the dotted (red) line in Fig. 2. It is also obvious from Fig. 2 that the average slope stiffness (dashed (blue) line) is incorrect for predicting small deflections relative to q_0.

4.1. Mesh Stiffness and Dynamic Models

This section demonstrates that for dynamic analyses the choice is not just whether to use $k_a(t)$ or $k_l(t)$ for the mesh stiffness representation in any of the numerous tooth mesh models in the literature. The dynamic models for gear vibration differ based on the choice of the mesh force representation.

The equation of motion for a gear pair with meaningful rotations and negligible translations subject to constant applied toque is

$$m_e\ddot{q}_m + F_m = \frac{T_1}{r_{b1}} = \frac{T_2}{r_{b2}}, \quad m_e = \frac{J_1 J_2}{r_{b2}^2 J_1 + r_{b1}^2 J_2}, \tag{5}$$

where $J_{1,2}$ are the mass moments of inertia for gears 1 and 2, respectively. q_m is the dynamic transmission error. Equation (5) does not yet choose how to model the mesh force nor which mesh stiffness method is used.

Use of Eq. (4) gives the mesh force $F_m = T_1/r_{b1} + k_l(t)(q_m - q_0(t))$. Substitution of this result into Eq. (5) gives the equation of motion as

$$m_e\ddot{q}_m + k_l(t)q_m = k_l(t)q_0(t). \tag{6}$$

Equation (6) is called the local slope model.

A common mesh force representation using the average slope mesh stiffness is [3, 4, 5, 6, 9, 19, 24, 25, 31]

$$F_m = k_a(t)(q_m - \epsilon(t)). \tag{7}$$

This representation of mesh force is illustrated by the dashed (blue) line in Fig. 2. For moderate and large amplitude vibrations where q_m substantially differs from q_0 this line can meaningfully differ from the exact mesh force (solid line), which raises doubt about its validity for dynamic analyses. Use of Eq. (7) in Eq. (5) gives

$$m_e\ddot{q}_m + k_a(t)q_m = \frac{T_1}{r_{b1}} + k_a(t)\epsilon(t). \tag{8}$$

We call Eq. (8) the average slope model.

The models in Eqs. (8) and (6) are not exhaustive in the literature on gear mesh models. Our purpose is to discuss the average and local slope mesh stiffnesses for dynamic analyses, not to review different mesh force models for gear dynamics.

The local slope model (Eq. (6)) is fundamentally different from the average slope model (Eq. (8)) due to the different representations of the mesh force in Eqs. (4) and (7). The difference in models is not only the choice of $k_a(t)$ versus $k_l(t)$. Considering how they are derived from use of Eq. (4) or (7) in Eq. (5), it is apparent that it is incorrect to exchange $k_l(t)$ for $k_a(t)$ in Eq. (6) and to exchange $k_a(t)$ for $k_l(t)$ in Eq. (8).

Both models are parametrically excited from fluctuations in the tooth mesh stiffness. These fluctuations can be considerably different, however, as can be seen from Figs. 5, 6, 8, 10, and 11. The models also differ in the applied excitation from the right-hand-sides of Eqs. (6) and (8). The local slope model has excitation from the product of the local slope stiffness and the static transmission error, which will generally consist of both mean and fluctuating components. For the average slope model the excitation consists of a constant mean load from the nominal mesh force and a fluctuating component from the product of the average slope stiffness and the unloaded transmission error. The fluctuating component of the dynamic excitation in this model vanishes for unmodified gear teeth where $\epsilon(t) = 0$.

Figure 12 compares the dynamic response from the local and average slope models for a gear pair with tooth surface modifications. The dynamic response is numerically calculated from Eqs. (6) and (8). Noticeable differences occur between the models. The models predict nearly 13% difference in natural frequency. The vibration amplitudes differ, particularly near resonances. The response amplitudes at the natural frequencies of each model (near 2500 Hz) differ by 10.4%. Similar differences occur at the resonances due to higher harmonics of excitation that occur below the natural frequency.

Figure 13 shows a comparison of the average and local slope models (calculated by direct numerical integration of Eqs. (6) and (8)) with experimental results from Ref. [34] for an unmodified gear pair. For this unmodified gear pair both models reasonably predict the natural frequency of the system and the nonlinear dynamic response for a wide range of mesh frequencies. The nonlinearity is from contact loss included in Eq. (6) and (8) where the mesh force vanishes if the teeth separate ($q_m < 0$). For this unmodified gear pair, the two models have small differences in the predicted vibration amplitudes, even though the stiffness fluctuations and dynamic excitations between each

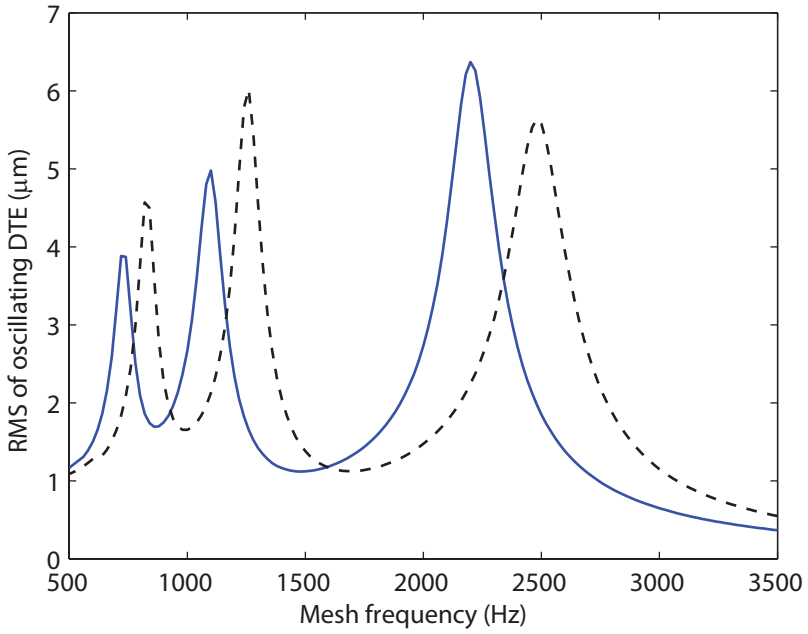

Figure 12: RMS of the oscillating component of dynamic transmission error for a ICR 1.37 gear pair at 170 Nm torque. Both gears have 10 μm of lead crown and 10 μm of linear tip relief (starting from 20.9 deg roll angle and extending to the tooth tip). The dashed (black) line is the local slope model in Eq. (6). The solid (blue) line is the average slope model in Eq. (8).

model differ.

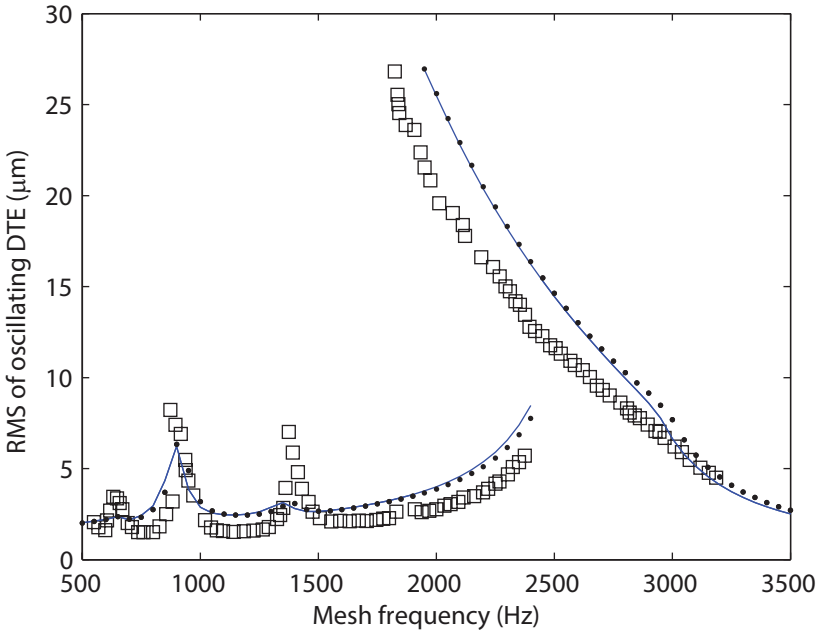

Figure 13: RMS of the oscillating component of dynamic transmission error for a ICR 1.37 unmodified gear pair at 170 Nm torque. The square markers are experimental results from Ref. [34]. The solid (blue) lines are from the average slope model. The dot markers are from the local slope model.

Figures 12 and 13 show that the two models may or may not give substantially different results. In choosing which to use for vibration analysis, however, the local slope model in Eq. (6) based on the mesh force model in Eq. (4) better represents the force versus deflection behavior compared to the average slope model based on Eq. (7).

4.2. Static Analysis and the Average Slope Approach

Before examining a system with multiple tooth meshes, we illustrate the appropriate use of average mesh stiffness for static analyses using the spur gear pair at 200 Nm torque with mesh stiffnesses in Fig. 11. Both gears have 10 μm lead crown and 10 μm of linear tip relief that starts at the pitch point (20.9 deg roll angle) and ends at the tooth tip. At mesh cycle 0.1 the average slope mesh stiffness $k_a = 143.3\ N/\mu m$ and the local slope stiffness

is $k_l = 178.2\ N/\mu m$ (Fig. 11). The nominal mesh force $F_m = T_1/r_{b1} = 200\ Nm/(0.07048\ m) = 2,837\ N$. Use of the average slope mesh stiffness gives the mesh deflection $q_m = F_m/k_a = 19.8\ \mu m$, which is precisely that given by the finite element/contact mechanics model. If the local slope mesh stiffness is used instead, a similar calculation gives $q_m = F_m/k_l = 15.9\ \mu m$, a -19.7% error compared to the finite element/contact mechanics model. Similar errors occur at other locations within a mesh cycle.

To illustrate the ideas above for systems with multiple tooth meshes, a three-gear idler system with only rotational degrees of freedom is used as an example. Although we illustrate the concepts using a purely rotational model, the results are valid for systems that include translations because the calculation of mesh stiffness using either the local or average slope approach is a static analysis conducted prior to and independently of the dynamic analysis that uses the mesh stiffness. Inclusion of bearing compliance and gear translations in a dynamic model does not affect the mesh stiffness. The system consists of three gears in mesh. The first gear (denoted by subscript "1") is the input gear with a fluctuating applied torque $T_1 = T_{10} + T_{1d}(t)$. The output gear is denoted by subscript "3", and it has torque T_3. The central idler gear is denoted by subscript "2". The gears have mass moments of inertia J_i and base radii r_{bi} $(i = 1, 2, 3)$. The mesh force between the i^{th} and j^{th} gears is F_{ij}, which is expressed in terms of the stiffnesses and deflections using Eq. (4) for each gear mesh. The equations of motion are

$$J_1\ddot{\theta}_1 + r_{b1}F_{12} = T_{10} + T_{1d}(t), \tag{9a}$$

$$J_2\ddot{\theta}_2 + r_{b2}F_{12} + r_{b2}F_{23} = 0, \tag{9b}$$

$$J_3\ddot{\theta}_3 + r_{b3}F_{23} = T_3, \tag{9c}$$

$$F_{12} = k_a^{(12)}(q_0^{(12)} - \epsilon_{12}) + k_l^{(12)}(q_{12} - q_0^{(12)}), \tag{9d}$$

$$F_{23} = k_a^{(23)}(q_0^{(23)} - \epsilon_{23}) + k_l^{(23)}(q_{23} - q_0^{(23)}), \tag{9e}$$

where the mean mesh deflections are $q_0^{(ij)} = r_{bi}\theta_{i0} + r_{bj}\theta_{j0}$ and the mesh deflections due to vibration or torque fluctuation are $q_{ij} = r_{bi}\theta_i + r_{bj}\theta_j$. Below we discuss the use of Eqs. (9) for static and dynamic analyses.

For static analysis of the idler gear system, the inertia terms in Eq. (9) vanish as does the input torque fluctuation $T_{1d}(t)$, and the objective is to determine the rotations θ_{i0} for specified steady applied torque T_{10}. The rotations θ_{i0} are relative to the unloaded state of the system. Constraining

the output gear to have no rotation ($\theta_3 = 0$), the component and matrix forms of Eq. (9) are

$$r_{b1} k_a^{(12)} (q_0^{(12)} - \epsilon_{12}) = T_{10}, \tag{10a}$$

$$r_{b2} k_a^{(12)} (q_0^{(12)} - \epsilon_{12}) + r_{b2} k_a^{(23)} (q_0^{(23)} - \epsilon_{23}) = 0, \tag{10b}$$

$$r_{b3} k_a^{(23)} (q_0^{(23)} - \epsilon_{23}) = T_3, \tag{10c}$$

$$\implies \mathbf{K}_a \mathbf{\Theta}_0 = \mathbf{T}_0, \quad \mathbf{\Theta}_0 = [\theta_{10}, \theta_{20}]^T, \tag{10d}$$

$$\mathbf{T}_0 = \left[T_{10} + r_{b1} k_a^{(12)} \epsilon_{12}, r_{b2} \left(k_a^{(12)} \epsilon_{12} + k_a^{(23)} \epsilon_{23} \right) \right]^T, \tag{10e}$$

$$\mathbf{K}_a = \begin{pmatrix} r_{b1}^2 k_a^{(12)} & r_{b1} r_{b2} k_a^{(12)} \\ r_{b1} r_{b2} k_a^{(12)} & r_{b2}^2 \left(k_a^{(12)} + k_a^{(23)} \right) \end{pmatrix}. \tag{10f}$$

The interpretation of the stiffness matrix $\mathbf{K}_a$ in Eq. (10f) is the same as the interpretation of k_a in Eq. (1). The mesh stiffness in Eq. (1) is, by definition, the average slope mesh stiffness. It relates the instantaneous force with the instantaneous total deflection, as shown in Fig. 2. The stiffness matrix $\mathbf{K}_a$ in Eq. (10d) plays the same role as k_a in Eq. (1). The elements of $\mathbf{K}_a$ in Eq. (10d) should be determined from the average slope method applied separately to each of the two mating gear pairs (that is, one average slope mesh stiffness analysis of gears 1 and 2 and a separate analysis of gears 2 and 3).

If the local slope method is used to calculate the mesh stiffness components in Eq. (10f), then the rotations calculated from Eq. (10d) for given applied torques would differ from the true rotations, as noted above for a single pair of gears.

Mesh stiffness calculation procedures in Refs. [31, 38, 39, 40], for example, use the average slope approach. These procedures are restricted to static analyses but inappropriate for dynamic analyses.

4.3. Dynamic Analysis and the Local Slope Method

For vibration analyses, or if one wants to calculate static ($\ddot{\theta}_i = 0$) deformations relative to the loaded state caused by input torque fluctuations, the rotations of interest are small fluctuating rotations $\theta_{id}(t)$ relative to the steady rotations θ_{i0} caused by the steady applied torque T_{10}, that is, we seek $\theta_{id} = \theta_i - \theta_{i0}$. Like above, we constrain the output gear to have no rotation ($\theta_3 = 0$). Use of the fact that the mesh forces from the steady rotations θ_{i0}

exactly balance the steady torques (i.e., Eqs. (10d)), the dynamic equations in Eqs. (9) are

$$J_1\ddot{\theta}_1 + r_{b1}k_l^{(12)}(q_{12} - q_0^{(12)}) = T_{1d}(t), \tag{11a}$$

$$J_2\ddot{\theta}_2 + r_{b2}k_l^{(12)}(q_{12} - q_0^{(12)}) + r_{b2}k_l^{(23)}(q_{23} - q_0^{(23)}) = 0, \tag{11b}$$

$$r_{b3}k_l^{(23)}(q_{23} - q_0^{(23)}) = T_3, \tag{11c}$$

$$\implies \mathbf{M}\ddot{\mathbf{\Theta}} + \mathbf{K}_l\mathbf{\Theta} = \mathbf{T}_d(t) + \mathbf{f}(t), \quad \mathbf{\Theta} = [\theta_1, \theta_2]^T, \tag{12a}$$

$$\mathbf{T}_d(t) = [T_{1d}(t), 0]^T, \quad \mathbf{f}(t) = \left[r_{b1}k_l^{(12)}q_0^{(12)}, r_{b2}\left(k_l^{(12)}q_0^{(12)} + k_l^{(23)}q_0^{(23)}\right)\right]^T, \tag{12b}$$

$$\mathbf{M} = \begin{pmatrix} J_1 & 0 \\ 0 & J_2 \end{pmatrix}, \quad \mathbf{K}_l = \begin{pmatrix} r_{b1}^2 k_l^{(12)} & r_{b1}r_{b2}k_l^{(12)} \\ r_{b1}r_{b2}k_l^{(12)} & r_{b2}^2\left(k_l^{(12)} + k_l^{(23)}\right) \end{pmatrix}. \tag{12c}$$

The steady torques do not appear because Eq. (12a) applies only for deformations relative to a loaded state. The elements of $\mathbf{K}_l$ in Eq. (12c) should be determined from the local slope method applied separately to each of the two mating gear pairs (that is, one local slope mesh stiffness analysis of gears 1 and 2 and a separate analysis of gears 2 and 3). The average slope method is incorrect for this type of vibration analysis, although its use is common (for example, Refs. [3, 4, 5, 6, 9, 10, 19, 24, 25]); it is only appropriate to capture gear deflections relative to the unloaded state.

The results calculated in this work using the local slope approach for high and low torque (Figs. 5 and 8(b)) and unmodified and modified (Figs. 5, 6, and 10(a)) gear teeth suggest rectangular wave approximations for mesh stiffness fluctuation may be valid in analytical studies on dynamic response like Refs. [1, 2, 5, 6, 7, 8, 11, 12, 13, 14, 15, 16, 17, 18, 19, 20, 21, 22, 23]. Note, however, that mesh stiffnesses can vary from rectangular waveforms near resonant gear speeds [29, 30] where the large vibration alters the dynamic mesh force, due to the presence of manufacturing and assembly errors [27, 28], and due to tooth damage [7, 32, 33, 40].

The presented results compare the local and average slope mesh stiffness approaches when calculating the total mesh stiffness of all contacting tooth pairs at a gear mesh interface. One must also choose between the two approaches when calculating the stiffness of the individual tooth pairs in mesh. In that case one uses the individual tooth forces instead of the total mesh force in Eqs. (1) and (2). This adjustment applies in models that account

for situations where two tooth pairs should be in contact, but only one tooth pair is actually in contact due to vibration, like Refs. [14, 22].

5. Conclusions

Spur gear tooth mesh stiffnesses calculated from the average slope approach differ substantially from those calculated by the local slope approach in both amplitude and shape for a wide range of applied torques. The differences between the two approaches are even greater when the gear teeth have tooth surface modifications. Local slope calculations of mesh stiffness show that profile modifications do not meaningfully change the stiffness amplitudes, although they alter the durations when one and two pairs of gear teeth are in contact. The average slope approach, however, predicts substantial mesh stiffness differences for gear teeth with profile modifications.

For models that calculate mean gear deflections relative to an undeflected state such as static windup, load sharing, and bearing forces under static conditions, the average slope approach stiffnesses should be used; the local slope method is incorrect. The local slope approach is preferred for dynamic gear models where the gears vibrate about a nominal static deflection. The question is more than just which stiffness to use in a particular vibration model, however; the vibration model itself differs based on which mesh stiffness representation one chooses. The physics/mechanics are incorrect if one simply exchanges the average slope stiffness for the local slope stiffness or vice versa in a given model. To use the recommended local slope stiffness appropriately for dynamic analyses, one must use the corresponding local slope gear vibration model. This model accurately represents the gear force-deflection behavior about a nominal load.

References

[1] R. W. Gregory, S. L. Harris, R. G. Munro, Dynamic behaviour of spur gears, Proceedings of the Institution of Mechanical Engineers 178 (1) (1963) 207–226.

[2] M. Benton, A. Seireg, Factors influencing instability and resonances in geared systems, ASME Journal of Mechanical Design 103 (2) (1981) 372–378.

[3] A. Kubo, Stress condition, vibration exciting force and contact pattern of helical gears with manufacturing and alignment error, ASME Journal of Mechanical Design 100 (1978) 77–84.

[4] R. Kasuba, J. W. Evans, An extended model for determining dynamic loads in spur gearing, ASME Journal of Mechanical Design 103 (2) (1981) 398–409.

[5] H. H. Lin, R. L. Huston, J. J. Coy, On dynamic loads in parallel shaft transmissions: Part I: Modelling and analysis, ASME Journal of Mechanisms, Transmissions, and Automation in Design 110 (2) (1988) 221–225.

[6] R. G. Parker, S. M. Vijayakar, T. Imajo, Non-linear dynamic response of a spur gear pair: Modelling and experimental comparisons, Journal of Sound and Vibration 237 (3) (2000) 435–455.

[7] S. Wu, M. J. Zuo, A. Parey, Simulation of spur gear dynamics and estimation of fault growth, Journal of Sound and Vibration 317 (2008) 608–624.

[8] T. Eritenel, R. G. Parker, Nonlinear vibration of gears with tooth surface modifications, ASME Journal of Vibration and Acoustics 135 (5) (2013) 051005.

[9] V. K. Tamminana, A. Kahraman, S. Vijayakar, A study of the relationship between the dynamic factors and the dynamic transmission error of spur gear pairs, ASME Journal of Mechanical Design 129 (1) (2007) 75–84.

[10] S. Li, A. Kahraman, Influence of dynamic behavior on elastohydrodynamic lubrication of spur gears, Proceedings of the Institution of Mechanical Engineers, Part J: Journal of Engineering Tribology 225 (8) (2011) 740–753.

[11] G. V. Tordion, R. Gauvin, Dynamic stability of a two-stage gear train under the influence of variable meshing stiffnesses, Journal of Engineering for Industry 99 (1977) 785–791.

[12] J. Lin, R. G. Parker, Mesh stiffness variation instabilities in two-stage gear systems, ASME Journal of Vibration and Acoustics 124 (1) (2002) 68–76.

[13] A. Kahraman, Dynamic analysis of a multi-mesh helical gear train, ASME Journal of Mechanical Design 116 (3) (1994) 706–712.

[14] G. Liu, R. G. Parker, Dynamic modeling and analysis of tooth profile modification for multimesh gear vibration, ASME Journal of Mechanical Design 130 (12), 121402.

[15] G. Liu, R. G. Parker, Nonlinear dynamics of idler gear systems, Nonlinear Dynamics 53 (4) (2008) 345–367.

[16] A. Kahraman, Load sharing characteristics of planetary transmissions, Mechanism and Machine Theory 29 (8) (1994) 1151–1165.

[17] P. Velex, L. Flamand, Dynamic response of planetary trains to mesh parametric excitations, ASME Journal of Mechanical Design 118 (1) (1996) 7–14.

[18] J. Lin, R. G. Parker, Planetary gear parametric instability caused by mesh stiffness variation, Journal of Sound and Vibration 249 (1) (2002) 129–145.

[19] V. K. Ambarisha, R. G. Parker, Nonlinear dynamics of planetary gears using analytical and finite element models, Journal of Sound and Vibration 302 (3) (2007) 577–595.

[20] R. G. Parker, X. Wu, Parametric instability of planetary gears having elastic continuum ring gears, ASME Journal of Vibration and Acoustics 134 (4) (2012) 041011.

[21] C.-J. Bahk, R. G. Parker, Analytical solution for the nonlinear dynamics of planetary gears, ASME Journal of Computational and Nonlinear Dynamics 6 (2) (2011) 021007.

[22] C.-J. Bahk, R. G. Parker, Analytical investigation of tooth profile modification effects on planetary gear dynamics, Mechanism and Machine Theory 70 (2013) 298–319.

[23] C. C. Zhu, X. Y. Xu, T. C. Lim, X. S. Du, M. Y. Liu, Effect of flexible pin on the dynamic behaviors of wind turbine planetary gear drives, Proceedings of the Institution of Mechanical Engineers, Part C: Journal of Mechanical Engineering Science 227 (1) (2013) 74–86.

[24] Z. Chen, Y. Shao, Dynamic features of a planetary gear system with tooth crack under different sizes and inclination angles, ASME Journal of Vibration and Acoustics 135 (3) (2013) 031004.

[25] Z. Chen, Y. Shao, D. Su, Dynamic simulation of planetary gear set with flexible spur ring gear, Journal of Sound and Vibration 332 (26) (2013) 7191–7204.

[26] P. Velex, M. Maatar, A mathematical model for analyzing the influence of shape deviations and mounting errors on gear dynamic behaviour, Journal of Sound and Vibration 191 (5) (1996) 629–660.

[27] X. Gu, P. Velex, On the dynamic simulation of eccentricity errors in planetary gears, Mechanism and Machine Theory 61 (2013) 14–29.

[28] X. Gu, P. Velex, A dynamic model to study the influence of planet position errors in planetary gears, Journal of Sound and Vibration 331 (20) (2012) 4554–4574.

[29] T. Eritenel, R. G. Parker, Three-dimensional nonlinear vibration of gear pairs, Journal of Sound and Vibration 331 (15) (2012) 3628–3648.

[30] T. Eritenel, R. G. Parker, An investigation of tooth mesh nonlinearity and partial contact loss in gear pairs using a lumped-parameter model, Mechanism and Machine Theory 56 (2012) 28–51.

[31] L. Chang, G. Liu, L. Wu, A robust model for determining the mesh stiffness of cylindrical gears, Mechanism and Machine Theory 87 (2015) 93–114.

[32] F. Chaari, T. Fakhfakh, M. Haddar, Analytical modelling of spur gear tooth crack and influence on gearmesh stiffness, European Journal of Mechanics A/Solids 28 (2009) 461–468.

[33] N. K. Raghuwanshi, A. Parey, Mesh stiffness measurement of cracked spur gear by photoelasticity technique, Measurement 73 (2015) 439–452.

[34] A. Kahraman, G. W. Blankenship, Effect of involute contact ratio on spur gear dynamics, ASME Journal of Mechanical Design 121 (1) (1999) 112–118.

[35] A. Kahraman, G. W. Blankenship, Effect of involute tip relief on dynamic response of spur gear pairs, ASME Journal of Mechanical Design 121 (5) (1999) 313–315.

[36] R. G. Parker, J. Lin, Mesh phasing relationships in planetary and epicyclic gears, ASME Journal of Mechanical Design 126 (2) (2004) 365–370.

[37] Y. Guo, R. G. Parker, Analytical determination of mesh phase relations in general compound planetary gears, Mechanism and Machine Theory 46 (12) (2011) 1869–1887.

[38] A. Palermo, D. Mundo, R. Hadjit, W. Desmet, Multibody element for spur and helical gear meshing based on detailed three-dimensional contact calculations, Mechanism and Machine Theory 62 (2013) 13–30.

[39] Z. Chen, Y. Shao, Mesh stiffness of an internal spur gear pair with ring gear rim deformation, Mechanism and Machine Theory 69 (2013) 1–12.

[40] Z. Chen, Y. Shao, Mesh stiffness calculation of a spur gear pair with tooth profile modification and tooth root crack, Mechanism and Machine Theory 62 (2013) 63–74.

[41] A. Fernandez del Rincon, F. Viadero, M. Iglesias, P. Garcia, A. de Juan, R. Sancibrian, A model for the study of meshing stiffness in spur gear transmissions, Mechanism and Machine Theory 61 (2013) 30–58.

[42] Y. Guo, R. G. Parker, Stiffness matrix calculation of rolling element bearings using a finite element/contact mechanics model, Mechanism and Machine Theory 51 (2012) 32–45.

[43] S. Vijayakar, A combined surface integral and finite element solution for a three-dimensional contact problem, International Journal for Numerical Methods in Engineering 31 (3) (1991) 525–545.

[44] C. G. Cooley, R. G. Parker, S. M. Vijayakar, A frequency domain finite element approach for three-dimensional gear dynamics, ASME Journal of Vibration and Acoustics 133 (2011) 041004.

[45] X. Dai, C. G. Cooley, R. G. Parker, Dynamic tooth root strains and experimental correlations in spur gear pairs, Mechanism and Machine Theory 101 (2016) 60–74.

[46] A. Singh, A. Kahraman, H. Ligata, Internal gear strains and load sharing in planetary transmissions: Model and experiments, ASME Journal of Mechanical Design 130 (7) (2008) 072602.